Current Applied Physics 86 (2026) 118–125

Contents lists available at ScienceDirect

Current Applied Physics

journal homepage: www.elsevier.com/locate/cap

Quantum dot–coated graphene/MoS_2 barristor for high-responsivity infrared photodetection

Jinsoo Shin [a], Do-Hyun Park [a,b], Inchul Choi [b], Jaeho Yu [b], Gil-Woo Lee [a], You-Shin No [a], Un Jeong Kim [c,*], Hyun-Jong Chung [a,b,**]

[a] Department of Physics, Konkuk University, Seoul, 05029, Republic of Korea
[b] A Barristor Company, Seoul, 05029, Republic of Korea
[c] Department of Physics, Dongguk University, Seoul, 04620, Republic of Korea

ARTICLE INFO

Keywords:
Barristor
Infrared photodetector
Schottky barrier modulation

ABSTRACT

Photodetectors operating at the eye-safe wavelength of 1550 nm are essential for applications such as LiDAR and optical communications; however, achieving high responsivity with atomically thin materials remains challenging. Here, we report a quantum dot-coated graphene/MoS_2 barristor photodetector enabling infrared detection via photogating-induced Schottky barrier modulation. Ligand-exchanged PbS quantum dots absorb 1550 nm light and transfer photoexcited carriers to graphene, modulating the Schottky barrier height (SBH) and inducing exponential current amplification. The device exhibits a current response of ~2000% and a responsivity up to ~780 A W^{-1} at a MoS_2 thickness of 4.5 nm, where a minimum SBH of ~0.246 eV is extracted from thermionic emission analysis. These results demonstrate that thickness-engineered Schottky barrier modulation provides an effective strategy for high-responsivity infrared photodetectors based on two-dimensional heterostructures.

1. Introduction

Photodetectors operating in the 1550 nm wavelength range are of particular technological importance for eye-safe applications such as LiDAR and optical communications, owing to reduced atmospheric attenuation and a higher maximum permissible exposure for the human eye [1–4]. These practical advantages have driven extensive efforts to develop compact, energy-efficient photodetectors exhibiting high responsivity in this technologically relevant near-infrared wavelength regime.

Graphene has been widely explored for photodetection because of its exceptionally high carrier mobility (reported up to ~200,000 cm^2 V^{-1} s^{-1}) and broadband optical response [5–10]. However, the absence of an intrinsic bandgap severely limits electrostatic current modulation in conventional graphene field-effect transistors, resulting in a low current on/off ratio (typically ~10–100) and substantial dark current [11–14]. To overcome this limitation without sacrificing graphene's mobility and Fermi-level tunability, Schottky barrier–based devices, commonly referred to as barristors, have emerged as an effective alternative [15–18]. In these architectures, the device current is governed by the Schottky barrier height (SBH) at a graphene/semiconductor interface and responds exponentially to barrier modulation, enabling current on/off ratios as high as ~10^5–10^6 and significantly enhanced sensitivity compared with graphene FETs [15–18].

Among two-dimensional semiconductors, MoS_2 is particularly attractive for barristor applications because it possesses a finite and thickness-dependent bandgap [19,20]. Monolayer MoS_2 exhibits a direct optical bandgap of ~1.8–1.9 eV as measured by photoluminescence (PL), which decreases toward ~1.2 eV in the multilayer or bulk limit due to interlayer coupling and the transition to an indirect bandgap, while angle-resolved photoemission spectroscopy (ARPES) reveals a clear thickness-dependent evolution of the MoS_2 band structure [19,20]. The electronic bandgap of monolayer MoS_2, as calculated by many-body theoretical analyses and supported by electrical transport trends, is ~2.4–2.5 eV for the direct K–K transition, substantially larger than the optical bandgap, and decreases toward the bulk limit consistent with quantum confinement effects [21]. This thickness-dependent electronic structure is expected to strongly influence band alignment

* Corresponding author.
** Corresponding author. Department of Physics, Konkuk University, Seoul, 05029, Republic of Korea.
E-mail addresses: ujjanekim@dongguk.edu (U.J. Kim), hjchung@konkuk.ac.kr (H.-J. Chung).

https://doi.org/10.1016/j.cap.2026.03.007
Received 12 February 2026; Received in revised form 9 March 2026; Accepted 9 March 2026
Available online 12 March 2026

and the effective SBH at graphene/MoS_2 junctions, providing a practical route for engineering barrier-controlled charge transport and photoresponse [15]. However, the intrinsic optical absorption of atomically thin MoS_2 at 1550 nm is relatively weak, making it insufficient as a standalone infrared absorber despite its favorable electronic properties [22–24].

Quantum dots (QDs) are an essential component of this platform, serving as efficient and spectrally tunable infrared absorbers [25–28]. In particular, PbS QDs exhibit strong absorption across the near-infrared region, including the 1550 nm band, and can transfer photoexcited carriers to graphene [25–27]. In practical eye-safe infrared photodetectors, high responsivity is a critical performance metric, as it enables low-power operation and efficient signal detection under weak illumination conditions [27,29,30]. While QD/graphene hybrid photodetectors have reported high responsivity, the enhancement is often indirect, relying on photogating effects and channel conductance modulation rather than efficient carrier injection [25–28]. In the present approach, photogating-induced charge transfer modulates charge transport at the graphene/MoS_2 junction, resulting in an enhanced current response associated with Schottky barrier modulation [15,16].

In this work, we report a QD-coated graphene/MoS_2 barristor photodetector operating at 1550 nm for infrared sensing. By combining ligand-exchanged PbS QDs with a thickness-engineered graphene/MoS_2 Schottky junction, we achieve a responsivity as high as ~780 A W^{-1} at an optimal MoS_2 thickness, while a fully processed, interface-cleaned device exhibits a responsivity of 21.6 A W^{-1} under standard illumination conditions. Thermionic-emission-based analysis reveals a minimum SBH of ~0.246 eV, indicating photogating-induced modulation of the SBH under infrared illumination. Importantly, we demonstrate that systematic control of the MoS_2 thickness offers an effective and previously underexplored strategy to engineer the SBH and optimize infrared photoresponse in barristor-based photodetectors. These results establish QD-coated MoS_2 barristors as a promising platform for high-responsivity, eye-safe infrared photodetectors based on two-dimensional material heterostructures.

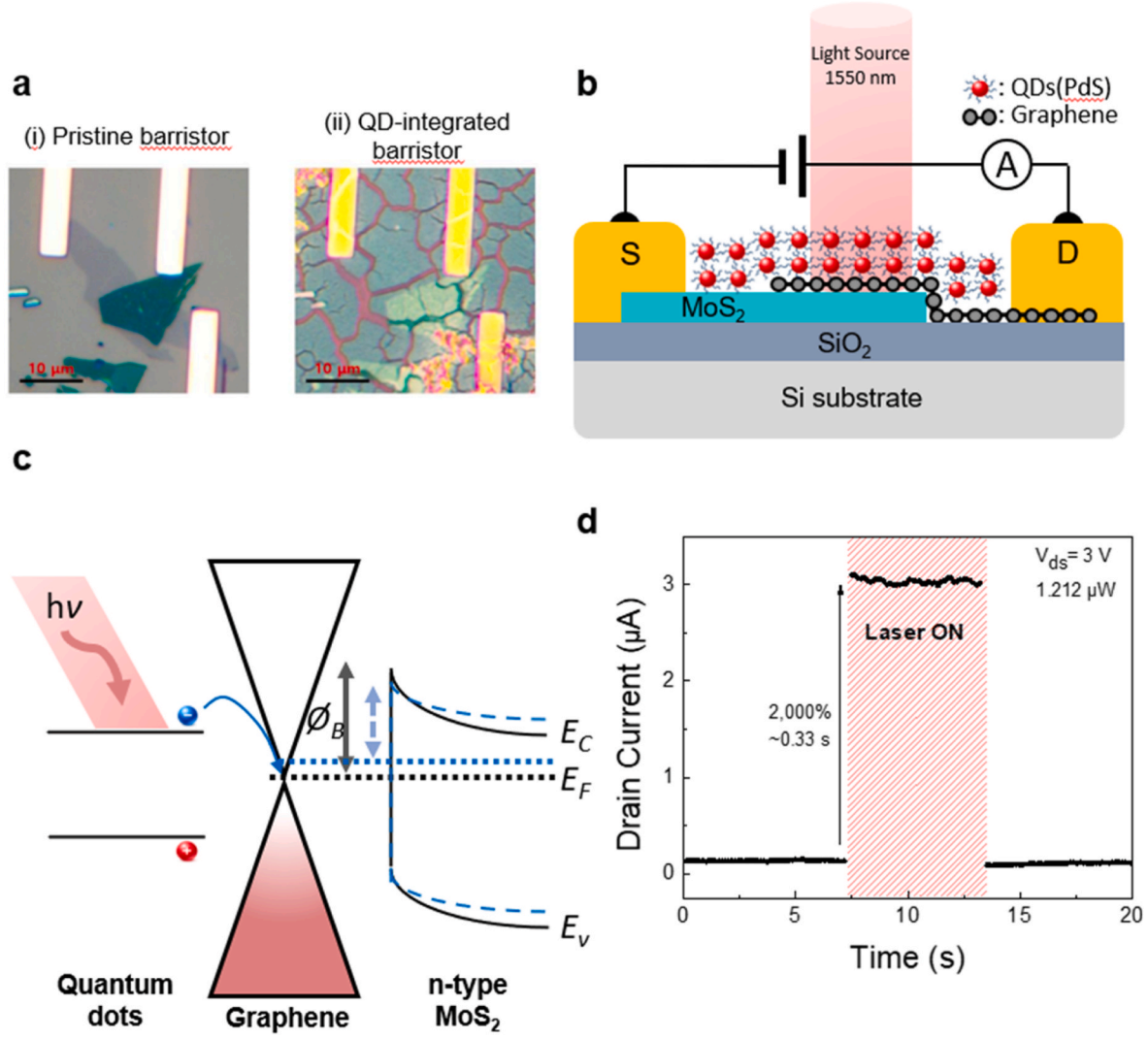

Fig. 1. Device structure, operating principle, and infrared photoresponse of the QD-coated barristor. (a) Optical images of the device: (i) pristine barristor without quantum dots (QDs) and (ii) QD-coated barristor after PbS quantum dot coating. (b) Schematic illustration of the QD-coated MoS_2 barristor photodetector under 1550 nm illumination, where photoexcited carriers in PbS QDs modulate the graphene Fermi level and the Schottky barrier at the graphene/MoS_2 junction. (c) Energy band diagram illustrating the photoresponse mechanism: incident infrared light generates electron–hole pairs in the QDs, and the photoinduced charge transfer to graphene alters the Schottky barrier height (SBH), resulting in an amplified current modulation. The blue dashed lines represent the band structure after electron injection into graphene. (d) Time-resolved drain current response of the QD-coated barristor under 1550 nm laser illumination (V_{ds} = 3 V, incident power = 1.212 μW), showing a pronounced current increase upon light exposure. (For interpretation of the references to colour in this figure legend, the reader is referred to the Web version of this article.)

2. Results and discussion

2.1. Results and discussion

The infrared photoresponse of the QD-coated MoS_2 barristor is attributed to photogating-induced Schottky barrier modulation at the graphene/MoS_2 junction, arising from photoexcitation in the PbS QDs [31]. Fig. 1a shows optical images of the fabricated device before and after PbS QD integration, the coating of PbS QDs on the device surface without measurable changes in the lateral device geometry. As illustrated schematically in Fig. 1b, the device consists of an n-type MoS_2 flake forming the source electrode and monolayer graphene serving as the drain electrode, thereby forming a vertical graphene/MoS_2 Schottky junction [32–34]. In this configuration, a positive drain bias corresponds to the forward-bias direction; a negative bias corresponds to the reverse-bias condition. Ligand-exchanged PbS QDs are coated on top of the graphene channel, where they function as an infrared photon-absorbing layer that induces photogating and couples optically generated carriers to the graphene/MoS_2 junction [35].

Under 1550 nm illumination, the PbS QDs absorb infrared photons with high efficiency and generate photoexcited charge carriers, which are subsequently transferred to graphene [25,27]. This charge transfer-induced photogating effect shifts the graphene Fermi level, thereby modulating the effective SBH at the graphene/MoS_2 interface, as depicted in the energy band diagram in Fig. 1c. The resulting SBH modulation induces a substantial variation in carrier injection across the junction, leading to a pronounced amplification of the modulation of the drain current.

This mechanism is directly manifested in the time-resolved drain current response measured at V_{ds} = 3 V (Fig. 1d), where a clear, reversible, and reproducible increase in drain current is observed upon laser illumination. The time-resolved current was recorded with an effective sampling interval of ap-proximately 0.33 s, and the photocurrent reaches a saturated level within this time scale after the laser is turned on. The current response, defined as the relative increase in drain current with respect to the dark current and expressed as $(I_{light} - I_{dark})/I_{dark}$, reaches a maximum value of approximately 2000%. This pronounced response under 1550 nm illumination confirms that the device

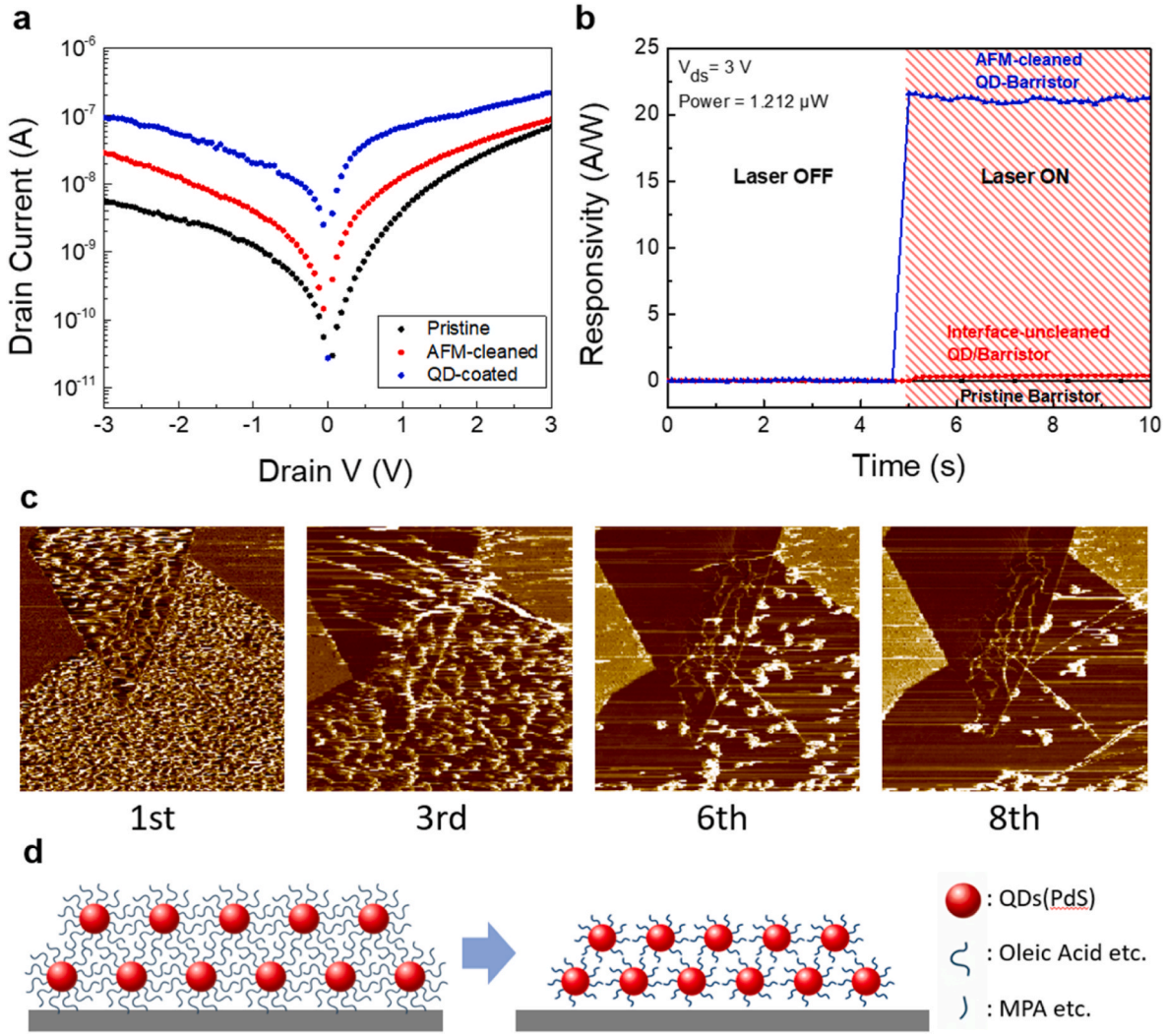

Fig. 2. Effect of interface cleaning and quantum dot integration on electrical and infrared photoresponse characteristics of the barristor. (a) Drain current–voltage (*I–V*) characteristics of the barristor measured after each fabrication step: before interface cleaning, after interface cleaning, and after PbS QD integration, showing a systematic increase in current due to reduced interfacial scattering and Schottky barrier modulation. (b) Time-resolved responsivity under 1550 nm laser illumination (V_{ds} = 3 V, incident power = 1.212 μW) for devices subjected to different interface conditions, including a bare barristor, an interface-unclean QD-barristor, and an interface-clean QD-barristor, highlighting the critical role of interface cleanliness in infrared photoresponse. (c) Lateral force microscopy (LFM) images acquired after successive AFM contact-mode scans (1st, 3rd, 6th, and 8th passes) during the interface-cleaning process, showing the progressive reduction of friction contrast at the graphene/MoS_2 interface. (d) Schematic illustration of the ligand exchange process in PbS QDs, where long-chain insulating ligands are replaced by shorter ligands, resulting in enhanced charge transport and improved electronic coupling between the QDs and graphene.

efficiently converts infrared photon absorption in the PbS QDs into an amplified electrical signal via Schottky barrier modulation, rather than through conventional photoconductive or bolometric mechanisms [25,27,31]. Given that Schottky barrier modulation is highly sensitive to interfacial charge states and local potential fluctuations, the quality of the graphene/MoS_2 interface is expected to play a critical role in determining the magnitude of the photoresponse.

To clarify the role of interface quality in this process, the electrical and photoresponse characteristics were systematically characterized after each fabrication step, namely after initial device fabrication, after AFM-based interface cleaning, and after QD integration, as summarized in Fig. 2. Fig. 2a presents *I–V* characteristics measured after each process step. Following AFM cleaning, the drain current exhibits a noticeable increase, which can be attributed to the removal of residual fabrication-induced contaminants remaining on the graphene surface [36]. These residues are known to induce unintentional p-type doping and carrier scattering in graphene; therefore, their removal leads to a partial recovery of intrinsic graphene transport properties and enhanced carrier injection across the graphene/MoS_2 Schottky junction [36]. After subsequent QD coating, a further increase in drain current is observed, consistent with electron transfer from PbS QDs resulting in n-type doping of graphene [25,28]. The systematic evolution of the *I–V* curves verifies that each fabrication step was successfully implemented and demonstrates that both interface cleaning and QD integration play critical roles in modulating charge transport across the Schottky junction.

The corresponding infrared photoresponse under 1550 nm illumination is shown in Fig. 2b. Measurements were performed at a drain bias of 3 V with an incident laser power of 1.212 μW. The bare MoS_2 barristor without QDs exhibits a negligible photoresponse, indicating that MoS_2 and graphene alone provide insufficient infrared absorption at this wavelength. In contrast, the interface-unclean QD-barristor shows a finite responsivity of approximately 0.4 A W^{-1}, demonstrating that QD integration enables infrared photodetection even in the absence of interface cleaning. Notably, when all fabrication processes are applied, including AFM-based interface cleaning and ligand-exchanged QD integration, the responsivity increases by nearly two orders of magnitude to 21.6 A W^{-1}. This comparison unambiguously demonstrates that a clean graphene/MoS_2 interface is essential for efficient charge transfer from the QDs to graphene and for enabling effective Schottky barrier modulation, thereby maximizing the infrared photoresponse of the barristor.

The responsivity was calculated as the photocurrent divided by the effective incident optical power, where the photocurrent is defined as the difference between the illuminated and dark drain currents. Specifically, the responsivity is given by Responsivity = $(I_{light} - I_{dark})/P_{eff}$ [25]. The effective incident power was determined as $P_{eff} = P_{laser} \times (A_{device}/A_{laser})$, where P_{laser} is the laser output power, A_{device} is the effective junction area, and A_{laser} is the laser spot area [25]. The laser spot size corresponds to a beam diameter of approximately 15 μm, yielding a laser spot area of approximately 176 μm^2. This definition provides a consistent and quantitative basis for comparing photoresponse among devices with different interface conditions.

Direct evidence for the effectiveness of AFM interface cleaning is provided by the LFM images shown in Fig. 2c [36]. As AFM contact-mode scanning is repeatedly performed, the area of the brighter regions in the images progressively diminishes indicating the gradual removal of polymer residues from the graphene/MoS_2 interface. This observation is fully consistent with the improvement in electrical characteristics observed in the *I–V* measurements and confirms that AFM cleaning effectively restores a cleaner and more spatially uniform graphene/MoS_2 interface.

In addition to interface cleaning, ligand exchange plays a critical role in achieving efficient infrared photoresponse, as illustrated schematically in Fig. 2d. Ligand exchange is required to transform colloidal QDs into electronically coupled solids suitable for optoelectronic devices [35]. The replacement of long-chain insulating ligands with shorter organic or inorganic ligands reduces the interdot spacing and lowers the interdot tunneling barrier, thereby enhancing charge transport within the QD film [35]. At the same time, ligand exchange effectively passivates surface trap states originating from the high surface-to-volume ratio of QDs, thereby suppressing nonradiative recombination pathways [35]. This process facilitates dense and uniform QD packing, resulting in compact films with reduced energetic disorder and improved electronic coupling to graphene, which is essential for efficient charge transfer and the realization of high responsivity.

The bias-dependent photoresponse provides direct insight into the carrier transport mechanism governing device operation. As shown in Fig. 3a–I–V characteristics measured under 1550 nm illumination exhibit a systematic and monotonic increase in drain current with increasing incident laser power. This trend is observed across the entire applied bias range, indicating that infrared illumination effectively modulates carrier injection and transport across the graphene/MoS_2 Schottky junction.

To further elucidate the bias asymmetry, time-resolved drain current measurements were performed at a fixed forward bias of 3 V under stepwise variation of the incident laser power (Fig. 3b). An enlarged view of the time-resolved trace highlighting the temporal spacing of the data points is provided in Fig. S3, showing that the photocurrent reaches saturation within approximately 0.41 s after illumination. Under forward bias, the drain current increases monotonically with increasing laser power, reflecting enhanced carrier injection across the Schottky junction induced by infrared-driven Schottky barrier modulation. In contrast, when the device is operated at a reverse bias of 3 V (Fig. 3c), the drain current also increases with laser power, but the magnitude of the photoresponse remains significantly smaller than that observed under forward bias, as further evidenced by the gate-controlled current modulation under reverse bias shown in Fig. S2. This behavior indicates that the on/off characteristics under forward and reverse bias are comparable and fall in the 10^1–10^2 range; however, the substantially larger current scale under forward bias results in a higher responsivity.

To quantitatively analyze this behavior, the reverse-bias current, where carrier transport remains Schottky-barrier-limited and minimally affected by series resistance, was analyzed using the thermionic emission (TE) model, which is appropriate for Schottky-barrier-limited transport [18,37]. According to the TE model, the current density is described by the following equation [18,37]:

$$J_{TE} = A^* T^3 \, exp\left(- q \frac{\Phi_B - \Delta\Phi_B(V)}{k_B T} \right) \tag{1}$$

In this equation, J_{TE} is the thermionic current density. T is the absolute temperature, and q is the elementary charge. k_B is Boltzmann's constant, and Φ_B is the SBH at zero bias. The exponential term accounts for the barrier height modulation due to surface charge, represented by $\Delta\Phi_B(V)$, where the current density is governed by thermionic emission over the Schottky barrier. In this framework, the effective Richardson constant is defined as:

$$A^* = \frac{q{k_B}^3}{\pi\hbar^3 {v_F}^2} \tag{2}$$

where $\hbar$ is the reduced Planck constant and v_F is the Fermi velocity of graphene. The barrier height shift $\Delta\Phi_B$ (V) arises from the modulation of the graphene Fermi level under reverse bias, reflecting the voltage-dependent charge redistribution across the Schottky junction, and is given by:

$$\Delta\Phi_B(V) = \frac{1}{2}\hbar v_F \sqrt{\frac{\pi\varepsilon_s\varepsilon_0 N_D (V_{bi} + V_R)}{2en_0}} \tag{3}$$

Here, ε_s is the dielectric constant of MoS_2 [38], ε_0 is the vacuum permittivity, N_D is the donor concentration in MoS_2, V_{bi} is the built-in

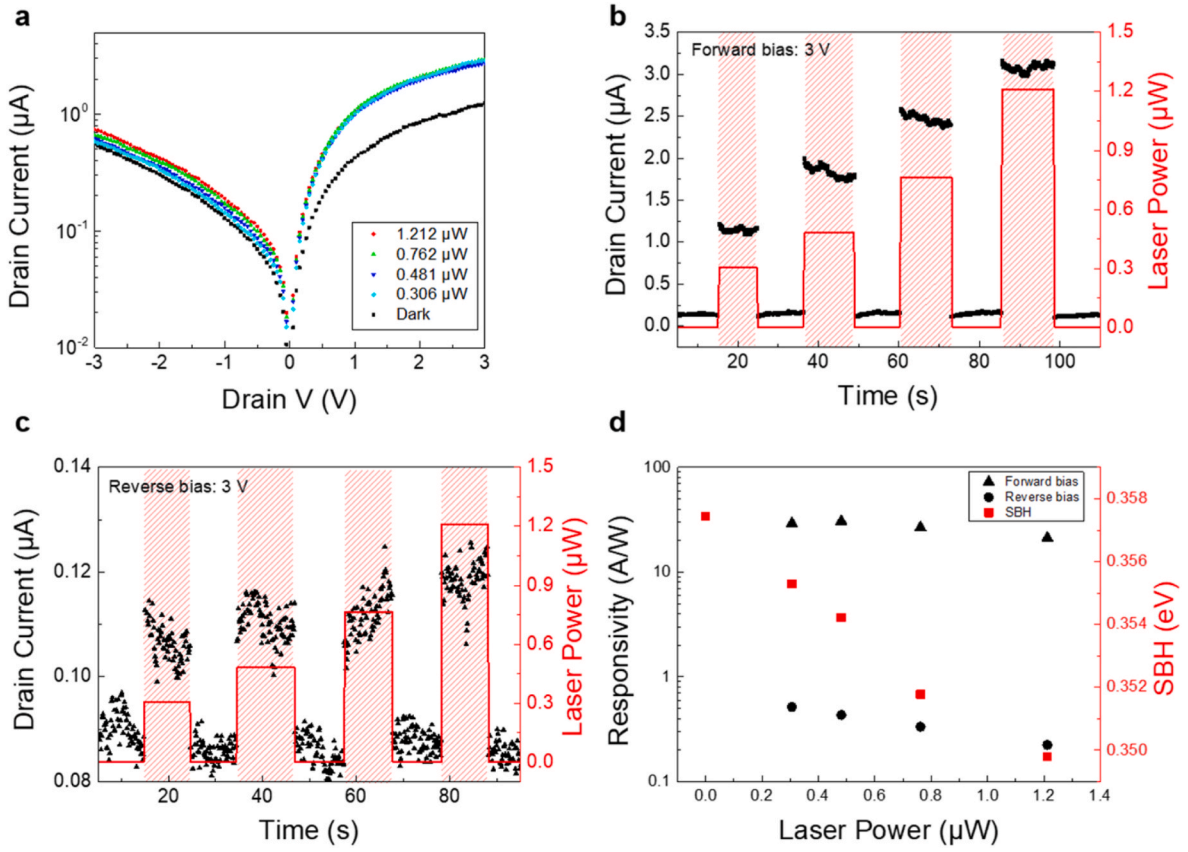

Fig. 3. Bias-dependent infrared photoresponse and Schottky barrier modulation in the QD-coated barristor. (a) *I–V* characteristics measured under 1550 nm illumination at different incident laser powers, showing a power-dependent increase in current due to photoinduced modulation of the graphene/MoS_2 Schottky junction. (b) Time-resolved drain current measured at a forward bias of 3 V under stepwise variation of the incident laser power, demonstrating a pronounced increase in photocurrent with increasing optical power. (c) Time-resolved drain current measured at a reverse bias of 3 V under the same illumination conditions, exhibiting a markedly weaker photoresponse compared to the forward-bias case. (d) Responsivity and extracted SBH as a function of incident laser power, revealing that the enhanced responsivity under forward bias correlates with a reduction in the effective SBH.

potential, V_R is the applied reverse bias (equivalent to the externally applied drain voltage, V_D), and n_0 is the equilibrium carrier density of graphene. These expressions account for the modulation of the SBH through changes in the graphene Fermi level under applied bias and infrared illumination.

Fig. 3d summarizes the responsivity and the extracted SBH as a function of incident laser power. Under forward bias, the responsivity reaches a maximum value of 30.7 A W^{-1} at an incident power of 0.481 μW and gradually decreases to 21.3 A W^{-1} at 1.212 μW, indicating partial saturation of Schottky barrier modulation at higher optical powers. In contrast, under reverse bias, the responsivity remains more than an order of magnitude lower, varying from 0.515 A W^{-1} at 0.306 μW to 0.2 A W^{-1} at 1.212 μW, consistent with carrier transport being primarily limited by the Schottky barrier. The clear correlation between the reduction in SBH and the enhancement of responsivity under forward bias confirms that Schottky barrier modulation is the dominant mechanism governing the infrared photoresponse.

Further insight into the photoresponse mechanism is obtained by examining the dependence on MoS_2 thickness, as exhibited in Fig. 4. Fig. 4a shows the dark *I–V* characteristics measured for barristors with different MoS_2 thicknesses, revealing systematic variations in both current magnitude and rectification behavior as the thickness increases. These results indicate that electrical transport across the graphene/MoS_2 junction is strongly influenced by thickness-dependent modulation of the Schottky barrier properties.

The corresponding time-resolved photoresponse measured under 1550 nm illumination is presented in Fig. 4b. A clear dependence of responsivity on MoS_2 thickness is observed, with the device incorporating a MoS_2 layer of approximately 4.49 nm exhibiting the strongest photoresponse, reaching a responsivity of ~780 A W^{-1}. Devices with thinner MoS_2 layers show comparatively weaker photoresponses, whereas increasing the MoS_2 thickness leads to an enhanced infrared detection performance.

Fig. 4c summarizes the responsivity extracted at forward and reverse biases of 3 V, together with the SBH obtained from thermionic emission fitting of the *I–V* characteristics in Fig. 4a. Notably, the MoS_2 thickness of 4.49 nm, which yields the maximum responsivity, corresponds to the minimum SBH of approximately 0.246 eV. This clear correlation suggests that the thickness-dependent infrared photoresponse is closely associated with Schottky barrier modulation, rather than being determined solely by optical absorption effects. While the forward-bias responsivity exhibits pronounced enhancement near the optimal thickness, the reverse-bias responsivity remains significantly lower, consistent with carrier transport being limited by the Schottky barrier.

The observed thickness dependence can be qualitatively interpreted in terms of the evolution of the electronic band structure of MoS_2 with thickness, which influences the effective Schottky barrier height at the graphene/MoS_2 junction. Monolayer MoS_2 exhibits a direct bandgap of approximately 1.8–1.9 eV, whereas multilayer and bulk MoS_2 show a reduced bandgap of approximately ~1.2 eV due to interlayer coupling [20]. This thickness-dependent reduction in bandgap is accompanied by changes in the band alignment at the graphene/MoS_2 interface, leading to a decrease in the effective Schottky barrier height. Similar behavior has been reported in graphene/WS_2 barristors, where a thickness-dependent reduction in the transition metal dichalcogenide bandgap leads to a systematic decrease in the Schottky barrier height,

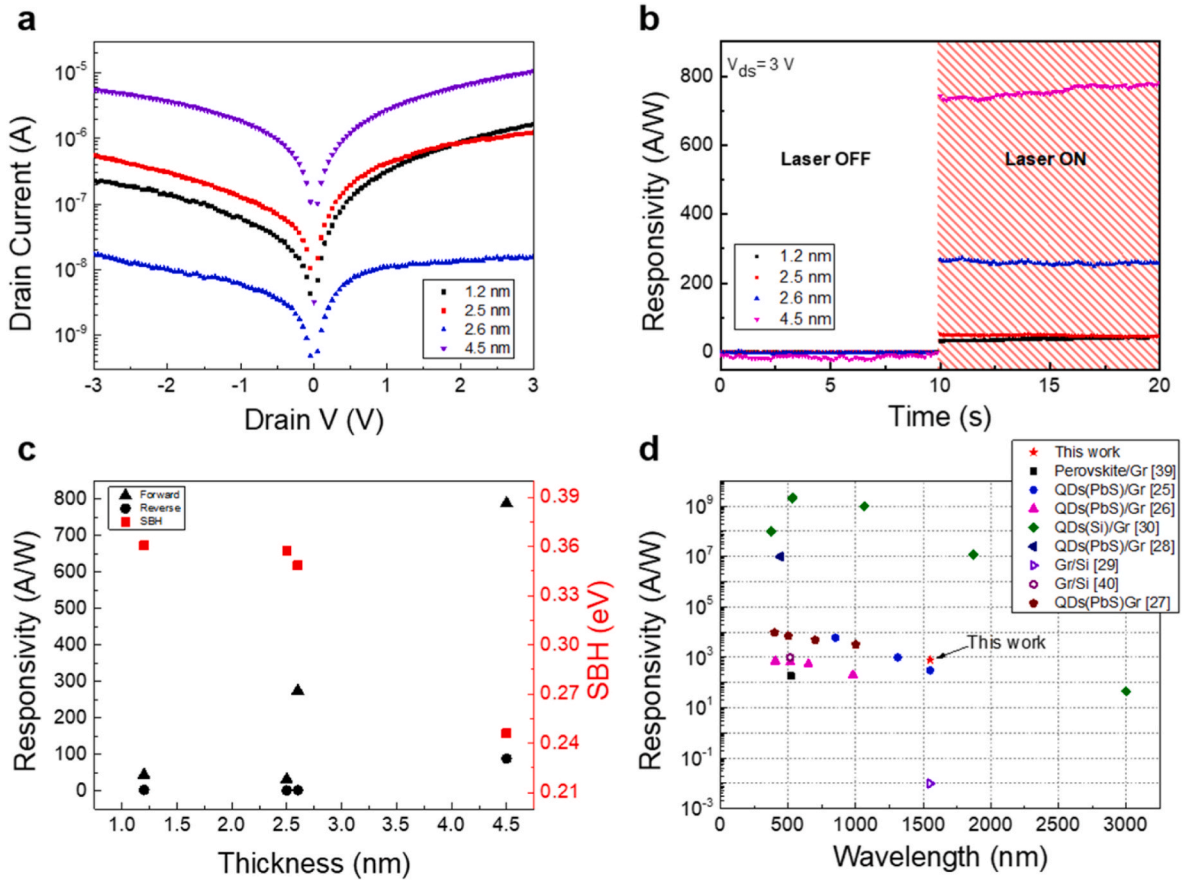

Fig. 4. Thickness-dependent electrical characteristics and photoresponsivity of the QD-coated MoS_2 barristor. (a) Dark *I–V* characteristics of the MoS_2 barristor measured for different MoS_2 thicknesses, showing a clear thickness-dependent modulation of the Schottky junction behavior. (b) Time-resolved responsivity under 1550 nm illumination (V_{ds} = 3 V) for devices with different MoS_2 thicknesses, highlighting a strong dependence of infrared photoresponse on the MoS_2 layer thickness. (c) Extracted responsivity under forward and reverse bias conditions, together with the corresponding SBH, as a function of MoS_2 thickness, indicating that the thickness-dependent photoresponse is closely correlated with Schottky barrier modulation. (d) Comparison of responsivity as a function of wavelength for this work and previously reported graphene-based photodetectors. Solid symbols denote devices incorporating QDs as light-absorbing layers, while open symbols represent QD-free devices. The present device exhibits competitive or enhanced responsivity over a broad spectral range compared with prior reports.

resulting in an increased on-current density [15]. A reduced Schottky barrier facilitates carrier injection across the junction, resulting in an increased on-current density and enhanced responsivity. These considerations indicate that MoS_2 thickness is a key parameter for tuning the effective barrier height and responsivity of MoS_2-based barristor photodetectors.

Finally, Fig. 4d compares the responsivity of the present device with that of previously reported graphene-based photodetectors over a wide spectral range [25–30,39,40]. Solid symbols represent devices incorporating QDs as light-absorbing layers, whereas open symbols denote QD-free devices. The QD-coated MoS_2 barristor reported here exhibits competitive or superior responsivity, particularly in the eye-safe infrared wavelength region around 1550 nm, underscoring the effectiveness of integrating QD-based infrared absorption with thickness-engineered Schottky barrier modulation in a barristor architecture.

3. Experimental methods

3.1. Device fabrication

Few-layer MoS_2 flakes were mechanically exfoliated from bulk crystals onto a highly doped Si substrate with a 90 nm SiO_2 layer. Monolayer graphene was mechanically exfoliated from natural graphite using adhesive tape [14] and identified by optical contrast and Raman spectroscopy (Fig. S1d) [41]. The graphene sheet was then transferred onto the selected MoS_2 flake via a wet-transfer method to form a graphene/MoS_2 heterostructure [42].

Source and drain electrodes were patterned by electron-beam lithography, followed by deposition of Ti/Au (20 nm/30 nm) using thermal evaporation and subsequent lift-off in acetone. Overall, a barristor device based on a van der Waals heterostructure of two-dimensional materials was fabricated.

3.2. AFM cleaning method

After device fabrication, resist and polymer residues remained on the sensing area even after acetone cleaning [36]. To remove these residual contaminants, the graphene surface, particularly the graphene/MoS_2 junction region, was mechanically cleaned using contact-mode atomic force microscopy (AFM) [36]. The cleaning was performed with a Park Systems NX-10 AFM operating in contact mode using a PPP-CONTSCR cantilever (NANOSENSORS™), applying a normal force of approximately 1 nN. The sensing region was repeatedly scanned (typically 5–10 times) to effectively sweep away residual polymers while avoiding damage to the underlying graphene or MoS_2.

The effectiveness of the mechanical cleaning process was confirmed by lateral force microscopy (LFM) imaging. As AFM contact-mode scanning was repeatedly performed, the area of the brighter regions progressively diminished, indicating the gradual removal of fabrication residues and improved surface uniformity [36]. The electrical characteristics before and after AFM cleaning further reflect changes associated

with the removal of p-doping residues from the graphene surface [36].

3.3. PbS quantum dot deposition and solid-state ligand exchange

PbS QDs dispersed in toluene (22.2 mg mL^{-1}) were spin-coated onto the fabricated graphene/MoS_2 barristor by dispensing 35 μL of the QD solution, followed by spinning at 2500 rpm for 25 s. To perform solid-state ligand exchange, the QD-coated device was immersed in a 30 mM tetrabutylammonium iodide solution in methanol for 1 min and subsequently rinsed with methanol to remove residual ligands and excess salts. This ligand exchange process replaces the native long-chain oleic acid ligands on PbS QDs with iodide-based ligands, thereby increasing the packing density of the QD film and improving charge transport within the QD layer and across the QD/graphene interface [35].

3.4. Photoresponse measurement

Photoresponse measurements were performed using a semiconductor parameter analyzer (Keithley 4200) at room temperature under ambient conditions. A continuous-wave 1550 nm laser was used as the infrared light source, generated using a VIAVI MAP-220C-A optical source equipped with a 1550 nm laser module, with a laser spot diameter of approximately 15 μm at the device plane. The drain current–voltage (*I–V*) characteristics were measured by sweeping the drain voltage from −3 V to +3 V with a step of 0.05 V under dark and illuminated conditions. Time-resolved drain current was recorded by periodically switching the laser on and off at a fixed drain bias, using a time step of approximately 0.1–0.2 s, with a longer integration time applied at low current levels to improve the signal-to-noise ratio.

4. Conclusion

In conclusion, we have demonstrated a QD-coated graphene/MoS_2 barristor photodetector enabling efficient and highly sensitive infrared detection at the eye-safe wavelength of 1550 nm. By integrating ligand-exchanged PbS QDs as an infrared-absorbing layer with a graphene/MoS_2 Schottky junction, the device directly converts photoinduced charge transfer into amplified electrical signals through SBH modulation. The pronounced current response and high responsivity observed under infrared illumination confirm that photogating-induced Schottky barrier modulation, rather than conventional photoconductive mechanisms, governs the photoresponse in this architecture.

Systematic investigations reveal that interface quality, bias polarity, and MoS_2 thickness collectively play critical roles in determining the magnitude of the infrared photoresponse. AFM-based interface cleaning is shown to be essential for maximizing charge transfer efficiency and effective Schottky barrier modulation, leading to a substantial enhancement in responsivity. Bias-dependent measurements, combined with thermionic emission–based analysis, establish a clear correlation between infrared illumination, SBH reduction, and current amplification, with forward-bias operation yielding a markedly stronger photoresponse than reverse bias. Furthermore, thickness engineering of MoS_2 provides an effective strategy for tuning the Schottky barrier, with an optimal MoS_2 thickness of approximately 4.49 nm yielding a minimum SBH of ~0.246 eV and a maximum responsivity of ~780 A W^{-1}.

These results highlight the effectiveness of integrating quantum-dot-based infrared absorption with thickness-engineered Schottky barrier modulation in a barristor platform. Beyond the specific PbS/graphene/MoS_2 system demonstrated here, the proposed design strategy is readily extendable to other two-dimensional semiconductors and quantum dot materials, offering a versatile pathway toward high-responsivity, low-power, and scalable infrared photodetectors. This work thus provides a foundation for the rational design of next-generation eye-safe infrared sensing devices based on two-dimensional material heterostructures.

Author contributions

Jinsoo Shin and Do-hyun Park contributed equally to this work. Jinsoo Shin conceived the concept and performed the experiments (Conceptualization; Investigation). Do-hyun Park performed the experiments, analyzed the data, and prepared the manuscript (Investigation; Formal Analysis; Writing – Original Draft). Inchul Choi assisted with experiments and data interpretation (Investigation). Jaeho Yu assisted with the experiments (Investigation). Gil-Woo Lee assisted with equipment operation and measurement support (Resources). You-Shin No provided experimental resources and measurement facilities (Resources). Un Jeong Kim contributed to manuscript revision and supervised the research (Writing – Review & Editing; Supervision). Hyun-jong Chung conceived the concept, supervised the overall research, and secured the funding (Conceptualization; Supervision; Funding Acquisition). All authors have read and agreed to the published version of the manuscript.

Statements and declarations

Do-hyun Park and Hyun-jong Chung declare financial interests in A Barristor Company. The remaining authors declare no competing financial interests.

Declaration of competing interest

The authors declare the following financial interests/personal relationships which may be considered as potential competing interests: Do-hyun Park and Hyun-jong Chung declare financial interests in A Barristor Company. The remaining authors declare no competing financial interests.

Acknowledgement

This research was supported by the Technology Development Program (RS-2024-00444122) funded by the Ministry of SMEs and Startups (MSS, Korea). This research was also supported by the National Research Foundation of Korea (NRF) (RS-2024-00343969, RS-2024-00454415, 2020R1A2C1003398) funded by the Korean Government (MSIT). Additional support was provided by the Dongguk University Research Fund of 2024 (S-2024-G0001-00023) and the Korea Basic Science Institute (National Research Facilities and Equipment Center) grant funded by the Ministry of Education (RS-2022-NF000887).

Appendix A. Supplementary data

Supplementary data to this article can be found online at https://doi.org/10.1016/j.cap.2026.03.007.

References

[1] Q. Wu, D. Xu, X. Ma, Z. Li, Y. Qu, Z. Qiao, G. Liu, Z. Zhao, L. Zeng, H. Chen, L. Li, L. Li, Study on 1550 nm human eye-safe high-power tunnel junction quantum well laser, Micromachines 15 (2024), https://doi.org/10.3390/mi15081042.
[2] M. Han, H.-S. Seo, B. Mheen, High-resolution and a wide field-of-view eye-safe LiDAR based on a static unitary detector for low-SWaP applications, Opt. Express 30 (2022), https://doi.org/10.1364/oe.468880.
[3] M. Akbulut, L. Kotov, K. Wiersma, J. Zong, M. Li, A. Miller, A. Chavez-Pirson, N. Peyghambarian, An eye-safe, SBS-free coherent fiber laser LIDAR transmitter with Millijoule energy and high average power, Photonics 8 (2021), https://doi.org/10.3390/photonics8010015.
[4] T. Sakimura, K. Hirosawa, Y. Watanabe, T. Ando, S. Kameyama, K. Asaka, H. Tanaka, M. Furuta, M. Hagio, Y. Hirano, H. Inokuchi, T. Yanagisawa, 155-μm high-peak, high-average-power laser amplifier using an Er,Yb:glass planar waveguide for wind sensing coherent doppler lidar, Opt. Express 27 (2019), https://doi.org/10.1364/oe.27.024175.
[5] M. Jin, H.K. Jeong, W.J. Yu, D.J. Bae, B.R. Kang, Y.H. Lee, Graphene oxide thin film field effect transistors without reduction, J. Phys. D Appl. Phys. 42 (2009), https://doi.org/10.1088/0022-3727/42/13/135109.

[6] K.I. Bolotin, K.J. Sikes, Z. Jiang, M. Klima, G. Fudenberg, J. Hone, P. Kim, H. L. Stormer, Ultrahigh electron mobility in suspended graphene, Solid State Commun. 146 (2008), https://doi.org/10.1016/j.ssc.2008.02.024.

[7] L. Wang, I. Meric, P.Y. Huang, Q. Gao, Y. Gao, H. Tran, T. Taniguchi, K. Watanabe, L.M. Campos, D.A. Muller, J. Guo, P. Kim, J. Hone, K.L. Shepard, C.R. Dean, One-dimensional electrical contact to a two-dimensional material, Science 342 (2013), https://doi.org/10.1126/science.1244358, 1979.

[8] A.B. Kuzmenko, E. Van Heumen, F. Carbone, D. Van Der Marel, Universal optical conductance of graphite, Phys. Rev. Lett. 100 (2008), https://doi.org/10.1103/PhysRevLett.100.117401.

[9] T. Mueller, F. Xia, P. Avouris, Graphene photodetectors for high-speed optical communications, Nat. Photonics 4 (2010), https://doi.org/10.1038/nphoton.2010.40.

[10] F. Xia, T. Mueller, Y.M. Lin, A. Valdes-Garcia, P. Avouris, Ultrafast graphene photodetector, Nat. Nanotechnol. 4 (2009), https://doi.org/10.1038/nnano.2009.292.

[11] D. Reddy, L.F. Register, G.D. Carpenter, S.K. Banerjee, Erratum: graphene field-effect transistors (Journal of Physics D: Applied Physics (2011) 44 (313001)), J. Phys. D Appl. Phys. 45 (2012), https://doi.org/10.1088/0022-3727/45/1/019501.

[12] A.H. Castro Neto, F. Guinea, N.M.R. Peres, K.S. Novoselov, A.K. Geim, The electronic properties of graphene, Rev. Mod. Phys. 81 (2009) 109–162, https://doi.org/10.1103/RevModPhys.81.109.

[13] K.S. Novoselov, Z. Jiang, Y. Zhang, S.V. Morozov, H.L. Stormer, U. Zeitler, J. C. Maan, G.S. Boebinger, P. Kim, A.K. Geim, Room-temperature quantum hall effect in graphene, Science 315 (2007), https://doi.org/10.1126/science.1137201, 1979.

[14] K.S. Novoselov, A.K. Geim, S. V Morozov, D. Jiang, Y. Zhang, S. V Dubonos, I. V Grigorieva, A.A. Firsov, Electric Field Effect in Atomically Thin Carbon Films, 2000.

[15] D.H. Choi, J.H. Lee, H.C. Kim, H.B. Lee, N.B. Jeoung, D.H. Park, H. Kim, S. H. Jhang, S.W. Lee, H.J. Chung, Engineering performance of barristors by varying the thickness of WS2, Curr. Appl. Phys. 17 (2017), https://doi.org/10.1016/j.cap.2016.10.015.

[16] H. Yang, J. Heo, S. Park, H.J. Song, D.H. Seo, K.E. Byun, P. Kim, I.K. Yoo, H. J. Chung, K. Kim, Graphene barristor, a triode device with a gate-controlled schottky barrier, Science 336 (2012), https://doi.org/10.1126/science.1220527, 1979.

[17] D.H. Shin, Y.G. You, S. Il Jo, G.H. Jeong, E.E.B. Campbell, H.J. Chung, S.H. Jhang, Low-power complementary inverter based on Graphene/carbon-nanotube and Graphene/MoS2 barristors, Nanomaterials 12 (2022), https://doi.org/10.3390/nano12213820.

[18] I. Choi, N. bong Jeong, M. Kim, J. Yu, H.J. Chung, Evolution of reverse-biased current of a barristor junction by varying temperature and barrier height of the junction, Adv. Electron. Mater. 8 (2022), https://doi.org/10.1002/aelm.202200761.

[19] K.F. Mak, C. Lee, J. Hone, J. Shan, T.F. Heinz, Atomically thin MoS2: a new direct-gap semiconductor, Phys. Rev. Lett. 105 (2010), https://doi.org/10.1103/PhysRevLett.105.136805.

[20] W. Jin, P.C. Yeh, N. Zaki, D. Zhang, J.T. Sadowski, A. Al-Mahboob, A.M. Van Der Zande, D.A. Chenet, J.I. Dadap, I.P. Herman, P. Sutter, J. Hone, R.M. Osgood, Direct measurement of the thickness-dependent electronic band structure of MoS2 using angle-resolved photoemission spectroscopy, Phys. Rev. Lett. 111 (2013), https://doi.org/10.1103/PhysRevLett.111.106801.

[21] H.J. Conley, B. Wang, J.I. Ziegler, R.F. Haglund, S.T. Pantelides, K.I. Bolotin, Bandgap engineering of strained monolayer and bilayer MoS2, Nano Lett. 13 (2013), https://doi.org/10.1021/nl4014748.

[22] A. Splendiani, L. Sun, Y. Zhang, T. Li, J. Kim, C.Y. Chim, G. Galli, F. Wang, Emerging photoluminescence in monolayer MoS2, Nano Lett. 10 (2010), https://doi.org/10.1021/nl903868w.

[23] G.A. Ermolaev, Y.V. Stebunov, A.A. Vyshnevyy, D.E. Tatarkin, D.I. Yakubovsky, S. M. Novikov, D.G. Baranov, T. Shegai, A.Y. Nikitin, A.V. Arsenin, V.S. Volkov, Broadband optical properties of monolayer and bulk MoS2, npj 2D Mater. Appl. 4 (2020), https://doi.org/10.1038/s41699-020-0155-x.

[24] A. Taffelli, S. Dirè, A. Quaranta, L. Pancheri, Mos2 based photodetectors: a review, Sensors 21 (2021), https://doi.org/10.3390/s21082758.

[25] L. Zheng, W. Zhou, Z. Ning, G. Wang, X. Cheng, W. Hu, W. Zhou, Z. Liu, S. Yang, K. Xu, M. Luo, Y. Yu, Ambipolar graphene–quantum dot phototransistors with CMOS compatibility, Adv. Opt. Mater. 6 (2018), https://doi.org/10.1002/adom.201800985.

[26] J. Zheng, W. Di, B. Bao, J. Lu, K. Yu, W. Wei, High-performance graphene–PbS quantum dots hybrid photodetector with broadband response and long-time stability, Appl. Phys. B 129 (2023), https://doi.org/10.1007/s00340-023-07988-y.

[27] A. Shultz, B. Liu, M. Gong, M. Alamri, M. Walsh, R.C. Schmitz, J.Z. Wu, Development of broadband PbS quantum dot/graphene photodetector arrays with high-speed readout circuits for flexible imagers, ACS Appl. Nano Mater. 5 (2022), https://doi.org/10.1021/acsanm.2c03839.

[28] Y.Q. Huang, R.J. Zhu, N. Kang, J. Du, H.Q. Xu, Photoelectrical response of hybrid graphene-PbS quantum dot devices, Appl. Phys. Lett. 103 (2013), https://doi.org/10.1063/1.4824113.

[29] M. Amirmazlaghani, F. Raissi, O. Habibpour, J. Vukusic, J. Stake, Graphene-Si schottky IR detector, IEEE J. Quant. Electron. 49 (2013), https://doi.org/10.1109/JQE.2013.2261472.

[30] Z. Ni, L. Ma, S. Du, Y. Xu, M. Yuan, H. Fang, Z. Wang, M. Xu, D. Li, J. Yang, W. Hu, X. Pi, D. Yang, Plasmonic silicon quantum dots enabled high-sensitivity ultrabroadband photodetection of graphene-based hybrid phototransistors, ACS Nano 11 (2017), https://doi.org/10.1021/acsnano.7b03569.

[31] S. Ahn, H. Chung, W. Chen, M.A. Moreno-Gonzalez, O. Vazquez-Mena, Optoelectronic response of hybrid PbS-QD/graphene photodetectors, J. Chem. Phys. 151 (2019), https://doi.org/10.1063/1.5132562.

[32] W. Zhang, C.P. Chuu, J.K. Huang, C.H. Chen, M.L. Tsai, Y.H. Chang, C. Te Liang, Y. Z. Chen, Y.L. Chueh, J.H. He, M.Y. Chou, L.J. Li, Ultrahigh-gain photodetectors based on atomically thin Graphene-MoS2 heterostructures, Sci. Rep. 4 (2015), https://doi.org/10.1038/srep03826.

[33] H. Tian, Z. Tan, C. Wu, X. Wang, M.A. Mohammad, D. Xie, Y. Yang, J. Wang, L. J. Li, J. Xu, T.L. Ren, Novel field-effect schottky barrier transistors based on graphene-MoS 2 heterojunctions, Sci. Rep. 4 (2014), https://doi.org/10.1038/srep05951.

[34] L. Xie, M. Liao, S. Wang, H. Yu, L. Du, J. Tang, J. Zhao, J. Zhang, P. Chen, X. Lu, G. Wang, G. Xie, R. Yang, D. Shi, G. Zhang, Graphene-contacted ultrashort channel monolayer MoS2 transistors, Adv. Mater. 29 (2017), https://doi.org/10.1002/adma.201702522.

[35] H.R. You, J.Y. Park, D.H. Lee, Y. Kim, J. Choi, Recent research progress in surface ligand exchange of PbS quantum dots for solar cell application, Appl. Sci. 10 (2020), https://doi.org/10.3390/app10030975.

[36] D.H. Park, Y.J. Cho, J.H. Lee, I. Choi, S.H. Jhang, H.J. Chung, The evolution of surface cleanness and electronic properties of graphene field-effect transistors during mechanical cleaning with atomic force microscopy, Nanotechnology 30 (2019), https://doi.org/10.1088/1361-6528/ab2cf6.

[37] P. Vigneshwara Raja, Forward and Reverse Current Transport Models in Schottky Barrier Diodes, n.d. https://hal.science/hal-04583749v1.

[38] A. Laturia, M.L. Van de Put, W.G. Vandenberghe, Dielectric properties of hexagonal boron nitride and transition metal dichalcogenides: from monolayer to bulk, npj 2D Mater. Appl. 2 (2018), https://doi.org/10.1038/s41699-018-0050-x.

[39] Y. Lee, J. Kwon, E. Hwang, C.H. Ra, W.J. Yoo, J.H. Ahn, J.H. Park, J.H. Cho, High-performance perovskite-graphene hybrid photodetector, Adv. Mater. 27 (2015), https://doi.org/10.1002/adma.201402271.

[40] X. Guo, W. Wang, H. Nan, Y. Yu, J. Jiang, W. Zhao, J. Li, Z. Zafar, N. Xiang, Z. Ni, W. Hu, Y. You, Z. Ni, High-performance graphene photodetector using interfacial gating, Optica 3 (2016), https://doi.org/10.1364/optica.3.001066.

[41] A.C. Ferrari, J.C. Meyer, V. Scardaci, C. Casiraghi, M. Lazzeri, F. Mauri, S. Piscanec, D. Jiang, K.S. Novoselov, S. Roth, A.K. Geim, Raman spectrum of graphene and graphene layers, Phys. Rev. Lett. 97 (2006), https://doi.org/10.1103/PhysRevLett.97.187401.

[42] S. Ullah, X. Yang, H.Q. Ta, M. Hasan, A. Bachmatiuk, K. Tokarska, B. Trzebicka, L. Fu, M.H. Rummeli, Graphene transfer methods: a review, Nano Res. 14 (2021), https://doi.org/10.1007/s12274-021-3345-8.